Nuclear Engineering and Technology 52 (2020) 1–13

Contents lists available at ScienceDirect

Nuclear Engineering and Technology

journal homepage: www.elsevier.com/locate/net

Review Article

A review on thermohydraulic and mechanical-physical properties of SiC, FeCrAl and Ti_3SiC_2 for ATF cladding

Bowen Qiu [a], Jun Wang [b], Yangbin Deng [c, *], Mingjun Wang [a], Yingwei Wu [a], S.Z. Qiu [a]

[a] Shaanxi Key Laboratory of Advanced Nuclear Energy and Technology, Shaanxi Engineering Research Center of Advanced Nuclear Energy, State Key Laboratory of Multiphase Flow in Power Engineering, Xi'an Jiaotong University, Xi'an City, 710049, China
[b] University of Wisconsin-Madison, Madison, WI, United States
[c] College of Physics and Optoelectronic Engineering, Shenzhen University, Shenzhen, 518060, China

ARTICLE INFO

Article history:
Received 19 April 2019
Received in revised form
17 July 2019
Accepted 29 July 2019
Available online 29 July 2019

Keywords:
ATF
SiC_f/SiC cladding
FeCrAl cladding
Ti3SiC2 cladding
Physical properties

ABSTRACT

At present, the Department of Energy (DOE) in Unite State are directing the efforts of developing accident tolerant fuel (ATF) technology. As the first barrier of nuclear fuel system, the material selection of fuel rod cladding for ATFs is a basic but very significant issue for the development of this concept. The advanced cladding is attractive for providing much stronger oxidation resistance and better in-pile behavior under sever accident conditions (such as SBO, LOCA) for giving more coping time and, of course, at least an equivalent performance under normal condition. In recent years, many researches on in-plie or out-pile physical properties of some suggested cladding materials have been conducted to solve this material selection problem. Base on published literatures, this paper introduced relevant research backgrounds, objectives, research institutions and their progresses on several main potential claddings include triplex SiC, FeCrAl and MAX phase material Ti3SiC2. The physical properties of these claddings for their application in ATF area are also reviewed in thermohydraulic and mechanical view for better understanding and simulating the behaviors of these new claddings. While most of important data are available from publications, there are still many relevant properties are lacking for the evaluations.
© 2019 Korean Nuclear Society, Published by Elsevier Korea LLC. This is an open access article under the CC BY-NC-ND license (http://creativecommons.org/licenses/by-nc-nd/4.0/).

1. Introduction

The concept of ATF originates from the nuclear disaster, which was as a subsequent consequence of earthquake and severe tsunami in Japan in 2011. Failure of cooling system failed at the beginning due to the station blackout accident (SBO). Without enough quality of coolant water, the fuel cladding finally reached the failure temperature and then lead to the reaction between coolant water and Zircaloy cladding. This dangerous oxidation reaction released immense heat and promoted the cladding temperature to higher level. What's more, hydrogen was also released by this reaction and accumulated to a dangerous point. As a consequence, a hydrogen explosion finally occurred and all the safety barriers were destroyed, fission products were released to the ocean [1,2]. This event with very low probability caused very serious discussions in the United States and soon extended to the world [2]. Again, the importance of the safety guarantee for nuclear plants is emphasized and promoted into a new high level. The point is that existing thermal hydraulic technology applicated in Light Water Reactors (LWRs) is near its inherent performance limit (the possibility of what happened in Japan is very low theoretically), its safety is difficult to be improved further by traditional methods under existing framework [3]. Therefore, Accident Tolerant Fuel concept was proposed and is becoming the most promising strategy to meet current challenges. The program on developing new nuclear fuel rod materials was initiated by the country's office of Nuclear Energy in DOE of United States and appropriated [4]. Funded by the U.S. DOE projects, this research is contributed by several campaigns, who is each led by a national laboratory in America currently [2,5–7]. Nuclear research industries, including General Electric, Westinghouse, General Atomic, AREVA, etc. and nuclear departments of several universities, including MIT, university of Purdue, university of Wisconsin-Madison, etc. are all participated in this new technology research [8–17].

It is known that Zirconium-water reaction played a very important role in fuel rod failure when the cladding temperature becomes very high. The immense oxidation heat promoted the temperature of the core and accelerated the reaction rate in return

* Corresponding author.
E-mail address: dengyangbin@szu.edu.cn (Y. Deng).

https://doi.org/10.1016/j.net.2019.07.030
1738-5733/© 2019 Korean Nuclear Society, Published by Elsevier Korea LLC. This is an open access article under the CC BY-NC-ND license (http://creativecommons.org/licenses/by-nc-nd/4.0/).

[18–20]. This vicious circle produced lot of hydrogen gas and then the explosion point would be reached. Therefore, to avoid this situation, much stronger oxidation resistance and very low, even none, combustible gas release rate in its oxidation reaction will be standards for the ATFs [21]. However, only having enhanced oxidation resistance is not enough for ATFs' goal. To allow tremendously longer existing operation time, stronger mechanical and better heat transfer performances are also required in ATF designs [22,23]. To achieve the requirements above, several new nuclear fuel rod materials, which have been studied or applied in other fields, are modified and proposed. For example, SiC, which is well used in steam generator, is proposed as an ATF cladding material candidate for its very strong antioxidant capability in steam environment [24–26]. However, be different from steam generator, the fuel cladding in-pile need to endure high radiation, hot water coolant washing and the mechanical interaction with pellet when the gas gap closes. Therefore, designers used a three layers structure, which has a ceramic matrix composites (CMC) SiC layer in the middle to resist the high hoop stress due to the contact, trying to make it applicable in light water reactor.

Looking back at the reasons to what happened in Fukushima Daichi nuclear plant is also a process of making requests on the new nuclear fuel with better accident tolerance [27–31]. This series of failure stages raised a claim that the next generation fuel rod systems should provide long enough coping time for nuclear reactor operators before the fuel degrades and fission products can break through the first barrier, the cladding, even in a very low probability of sever accident with no active cooling action. To approach this effect, passive cooling system design and high-performance fuel rod materials, which can provide sufficient cooling capability and stable working performance respectively in a certain range under accident conditions, are combined to prevent the core from reaching the failure condition in long enough time for operation [11,32]. This paper focuses on the directed efforts of the researches about physical properties of potential materials for ATF cladding.

To reduce the fabrication cost, ATFs are desired to be applied in existing nuclear reactor directly. Thus, fuel rod improvement without big geometry changes are preferred in current researches. Generally, there are three ways have been considered in enhancing the performance of the claddings, which includes: 1) developing new non-zirconium cladding [22,23]; 2) enhancing current zircaloy cladding [23,33,34]; 3) coating the existing zircaloy cladding with antioxidation material on the surface [9,23,35]. There are some differences between these thoughts and result in different consequences. For example, coating the zircaloy cladding will inherit the mechanical properties of zircaloy cladding in general while a new non-zirconium cladding material, such as ceramic matrix composites (CMC) SiC cladding, will lead to a totally different mechanical mechanism. In any case, the primary objective of these methods is to solve the oxidation reaction and hydrogen generation problems at high temperature. In contrast, approaches for improving the pellets' performance seem to be less differential. Better thermal performance under high burnup condition is the main goal for ATF pellet materials. The capability of retaining fission products, if it's feasible, can also promote the accident tolerant ability of the fuel pellet during accident conditions.

At present, universities [36–42], national labs [12,43–50], relevant industries [32,51,52] and other cooperators are working together on this promising technology no matter via experiments or simulations. What's more, a leading test assembly is going to be applied in a commercial reactor by 2022 [2,5–7]. With no doubt, applying ATF designs in LWR is still facing lots of problems. The first is that many in-pile or out-pile physical properties need to be confirmed via experiments. In fact, many researchers have been conducting relevant researches, which are also what we want to review in this paper. Relevant code tools that can be trusted for assessing the performance of the ATF candidate designs under different conditions are still vacant. What's more, a new material would bring its particular issues, like the dissolution behavior of SiC in water coolant environment for LWR under normal condition. In a word, these designs still need to be assessed by computer codes, validated in tests and furtherly modified before their practical application.

2. Summary of the physical properties of three potential ATF cladding materials

2.1. Full SiC_f/SiC cladding

2.1.1. Overview

Small neutron absorption cross sections, much higher oxidation resistance, chemical inertness, much higher melting point, lower irradiation growth and stabilization in nuclear waste, SiC has lots of advanced performances compared with traditional zircaloy cladding [21,53,54] and these advantages make it very attractive when it was considered as an ATF cladding material. In fact, the using of this material can data back to 1960s when it was used in high-temperature gas reactors for its outstanding antioxidation [24,25]. Now the researches want to extend the use of this material to fuel cladding material. Moreover, this material is also considered as matrix material in fully ceramic micro-encapsulated (FCM) fuel for its minimal irradiation swelling rate [11,55].

To evaluate its feasibility in ATF field, Oak Ridge National Laboratory (ORNL) [56–59], MIT [60,61] and many other research institutions all around the world have conducted a lot of in-pile and out-pile experiments to evaluate its application possibility in LWR. For example, Oak Ridge National Laboratory (ORNL) has performed high-temperature oxidation test on Chemical Vapor Deposition (CVD) SiC specimens in severe accident test station (SATS), these specimens were exposed to steam at high temperature range from 1473 K to 1973K resulting that the inherent characteristic of SiC can greatly enhance fuel integrity under accident conditions [57]. Researchers from MIT simulated and evaluated the behavior of SiC_f/SiC cladding under normal conditions with modified FRPCON code based on the experimental data from their in-pile tests. What's more, new simulation tools, such as BISON, is under development to simulate this new cladding under normal and accident conditions.

In general, two classes are proposed in SiC cladding designs including full ceramics and metal-assisted ceramics, which can also be subdivided into composite, composite-monolith (Duplex structure), monolith-composite-monolith (Triplex structure) for full ceramics design and metal-composite (Duplex structure), composite-metal-composite (Triplex structure) for metal-assisted ceramics design [58–65]. It should be noted that there are still no standards for the designs or manufacturing of the SiC fiber-reinforced cladding, the standards are under development. The object reviewed in this paper is limited in full SiC fiber-reinforced cladding. The general manufacturing steps for no matter what designs are as follows [56]:

a) Depending on the architecture of the SiC tubes, SiC fibers are blended into the tubes by different methods, including filament winding and braiding;
b) Through CVD method, an interphase layer is added;
c) SiC matrix is add by chemical vapor infiltration (CVI);
d) The environment barrier coating (EBC) may be added by different techniques.

Refer to the introductions above, fibers, interphase layer, matrix

and EBC constitute the full SiC_f/SiC cladding, these four parts are to provide different functions specifically.

No matter the triplex or the duplex structure, the SiC composite layer is deposited into matrix to enhance the cladding mechanical performance. The SiC/SiC composites reviewed in this paper are limited to continuous SiC fiber-reinforced composites with fully crystalline SiC material. These nuclear-grade SiC fibers include Hi-Nicalon type-S (HNS) and Tyranno SA3 [66–68]. These fibers can provide similar mechanical performance but obviously different thermal performance [62,63,69]. This paper will emphatically introduce the SiC cladding with Nicalon and HNS fibers.

Because the fiber can provide the best mechanical performance in the fiber axis direction, the volume of the SiC fibers and the way to build the composite layer deeply affect the finial performance of the SiC cladding. At present, braiding, no matter 2 directions (2-D) or 3 directions (3-D), is becoming popular due to its better damage resistance and conformability. Fig. 1 shows three typical examples of the fiber architecture. Therefore, the complex level of the SiC cladding simulation becomes higher by introducing the fiber material kinds and its architectures.

Even though SiC/SiC composites have excellent mechanical properties and damage tolerance, enough bounding strength is still needed when its normal functions are enabled. Therefore, the interphase, which combines the matrix and the fiber composite layer by providing bonding strength, is added via CVD technique typically. The parameters of the interphase, such as its thickness, will affect the cladding performance refer to previous report, but no systematic evaluation on the tubular SiC_f/SiC materials has been reported.

As a relatively matured technology to get a long enough SiC thin tube, it seems that CVI is the most stable and reliable way to produce the SiC matrix with very high purity and low porosity in large scale. However, a large facility is needed if the tube length wants to achieve the LWR application requirements, also it will take more time on the deposition process for low internal porosity of the tube. There are some research institutions have the capability to produce SiC long tubes (about 1 m) so far [62,71]. The other method to produce the tube is so called NITE (nano-infiltration and transient eutectic phase) process. However, it contains secondary phases attributed to the oxide additives, the hot water or steam in normal operation and high temperature steam accident conditions can lead to significant dissolution of the SiC matrix material, it is a critical challenge for its LWR application [72,73].

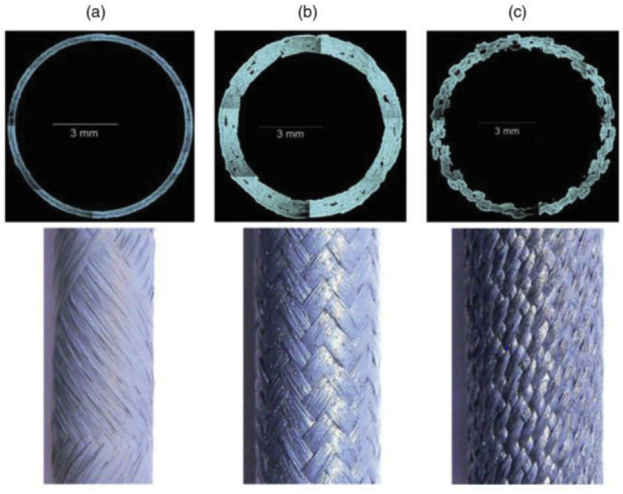

Fig. 1. Three typical examples of SiC fiber architecture of CVI SiC tube. Reprint from Sauder 2014 [70].

It was reported that the SiC has dissolution phenomenon at a higher rate compared with the oxidation rate of zircaloy cladding under normal condition [72–74]. The reports showed that the dissolution began at the grain boundary and occurred throughout the surface, then the grain became thinner with the dissolution occurs and finally detached from the surface. Additional, neutron irradiation will accelerate this process which depends on DPA, oxygen content and other factors [74]. The details will be described in following sections. For this reason, EBC on outer surface for protection in normal operation conditions is one of the possible solutions, which is also a familiar method that applicated on turbines. But the coating technology on SiC composite cladding is still immature, the coating materials or the coating technique still cannot reach a consensus currently [75,76].

2.1.2. Thermal conductivity

Thermal conductivity along the matrix thickness is the key parameter for heat transfer, a higher thermal conductivity results in a lower fuel rod temperature and smaller temperature gradient. Many research institutions have conducted experiments to measure this parameter, including MIT and ORNL. It's known that the neutron irradiation has influence on the thermal conductivity, but there is no reliable data of thermal properties on irradiated SiC tube that can found in publications [56]. Therefore, currently the relative parameters were obtained from the plate specimens when it's needed in simulations.

According to MIT's reports [60], the in-pile thermal conductivity correlation of CVI matrix SiC cladding with Nicalon fibers has been established based on experimental data from Maruyama and Harayama [77] as shown in Eq. (1).

$$K_{clad} = K_{sat} \cdot \left(\frac{(d + d_0)}{d_{sat}} \right)^{-0.4} \tag{1}$$

where k_{clad} is thermal conductivity of SiC cladding (W/m·K); k_{sat} is the thermal conductivity when the neutron fluence reaches the saturation DPA, which is regardless of temperature and set as 20 W/m·K; d is cumulative cladding neutron irradiation influence (DPA) which is set as 1 DPA; d_{sat} the saturation neutron influence, which is set as 1 DPA in their paper; d_0 is defined as:

$$d_0 = d_{sat} \cdot \left(\frac{k_{sat}}{k(T)} \right)^{2.5} \tag{2}$$

where $k(T)$ is the thermal conductivity of the SiC tube which is dependent on temperature by Eq. (3).

$$K_T = 8 \times 10^{-6} \cdot T_{lad}^2 - 0.02 \cdot T_{clad} + (k_{rt} + 26.4) \tag{3}$$

The researchers compared this model with limited available data, there is a good agreement between them, even though the estimation on the saturation DPA and the saturation temperature was conservative. In fact, in Snead's report [78,79], the saturation conductivity was about 10 W/m·K.

In ORNL's report [56], the researches followed Snead's conclusion [79] and defined the thermal resistivity as Eq. (4):

$$\frac{1}{K_{\mathrm{rd}}} = \frac{1}{K_{irr}} - \frac{1}{K_{non-irr}} \tag{4}$$

where $\frac{1}{K_{\mathrm{rd}}}$ is thermal resistivity from the radiation produced defects (m·K/W), $\frac{1}{K_{irr}}$ and $\frac{1}{K_{non-irr}}$ is the irradiated and nonirradiated thermal resistivity respectively. This parameter is material dependent and

the corresponding triplex tube cladding would be affected by the performance of the monolithic layer for their volume fraction. For now, relative data is very limited, future work on this topic is very needed.

2.1.3. Specific heat

Because the effect of the presence of a carbon interphase [69] is negligible, the specific heat of the SiC cladding is often assumed as same as that of monolithic SiC with very high purity. Moreover, it is clear that the irradiation effects on specific heat can also be neglected. Therefore, based on the review work of Snead et al. [79], the correlation of the specific heat that can be used in simulation is as Eq. (5):

$$C_p = 925.65 + 0.3772T - 7.9259 \times 10^{-5}T^2 - \frac{3.1946 \times 10^7}{T^2} \tag{5}$$

where C_p is the temperature-dependent specific heat (J/kg·K); T is the temperature (K).

2.1.4. Thermal expansion

The cladding thermal expansion is very important at the beginning of life, higher thermal expansion will lead to higher hoop strain of the cladding and greater gap thickness between the cladding and pellets, which results in higher thermal resistivity of the gap. The gap thickness can affect the thermal performance of the whole fuel rod significantly.

In MIT and other institutions' reports [60,80,81], the thermal expansion coefficient of the SiC composites is weakly dependent on temperature and generally $2-5 \times 10^{-6}$ 1/K for different types of the fibers and the architecture methods. According to their reports, the difference between swelling parallel and perpendicular is not apparent and the identical coefficient in each direction is assumed as 3×10^{-6} 1/K.

Since the coefficient of thermal expansion of SiC cladding tube is rare so far in published data, general treatment in simulation for now is to expect that the tubes have similar CTEs compared with the plate SiC materials for the similar microstructure. Therefore, according to the study of Katoh et al. the CTE of CVI SiC composite plates can be obtained by Eq. (6) as follows:

$$\alpha = 0.7765 + 1.435 \times 10^{-2}T - 1.2209 \times 10^{-5}T^2 + 3.8289 \times 10^{-9}T^3 \tag{6}$$

where α is the thermal expansion coefficient (10^{-6}/K); T is the temperature (K) from 293 K to 1273 K. The in-pile experiments for HNS fiber-reinforced CVI SiC composite plates by ORNL in the High Flux Isotope Reactor (HFIR) showed that the effect of irradiation on the CTE was not important and this conclusion is consistent with the previous work by Katoh et al. [69].

2.1.5. Young's modulus

In elastic phase, Young's modulus can describe the material's mechanical response to external tension or compression stress. However, for composite material specimen, this behavior becomes complex because of the fiber. The types of fibers and matrix, void fraction, load direction and the architecture pattern are all factors that can affect the final mechanical performance of the SiC cladding.

David et al. from MIT summed up previous works on SiC composite plate specimens from Miriyala et al. and Jones et al. [80,82] and obtained a fitting correlation as Eq. (7),

$$E_T = -4 \times 10^7 T + 1.62 \times 10^{11} \tag{7}$$

where E_T is the un-irradiated Young's modulus (Pa); T is the temperature (K). Moreover, it's noted that these specimens showed slightly decrease in Young's modulus under in-pile environment and Eq. (7) was modified as shown in Eq. (8):

$$E_{ir} = E_T \cdot \left(1 - 0.4 \cdot \left(1 - e^{-0.15 \times DPA}\right)\right) \tag{8}$$

The correlation above is based on the estimation of experiment results of Nicalon fibers under in-pile conditions and assumed that it was identical in each direction. As a newer type of SiC fiber, Hi-Nicalon type-S (HNS) is more broadly used in recent researches. In the study of Rohmer et al. [83], the in-pile and out-pile mechanical properties of CVI/HNS SiC cladding tube were systematically reported and the fiber architecture was 30°. According to their report, the Young's modulus of the cladding tube in axial direction was 232.2 GPa and 157.5 GPa in hoop direction. Even though resent studies [84–86] showed that the irradiation effect on mechanical properties of CVI/HNS tube cladding will not lead to notable degradation under normal conditions, it should be noted that after be irradiated in HFIR (up to 11.6 DPA at temperature of 280–340 °C), the Young's modulus had a reduction about 18% (from 255 GPa to 210 GPa) [84].

2.1.6. Ultimate tensile strength and strain

As a brittle material, the plastic strain term is little before it fails, thus the ultimate tensile strength was assumed be equal to the yield strength in David's work. He proposed a fitting correlation for CVI/Nicalon cladding based on the experiment data from Miriyala et al. and Jones et al. [80,82] as Eq. (9) and Eq. (10) shows.

$$S_T = 2.66 \times 10^4 \cdot T + 2 \times 10^8 \tag{9}$$

$$S_{ir} = S_T\left(1 - 0.4\left(1 - e^{-0.15 \times DPA}\right)\right) \tag{10}$$

where S_T is the un-irradiated UTS (Pa); S_{ir} is the irradiated UTS (Pa); T is the temperature (K); DPA was the neutron influence. It should be noted that the cladding with Nicalon fibers is highly dependent on neutron influence and the decrease of the UTS can be up to 40%. However, refer to Hinoki's study, for higher grade fiber, HNS, the irradiation will increase its UTS and this agreed with relevant later works.

According to resent researches [87], it was found that the fiber orientation has important effect on the UTS. There is no available experiment data for Nicalon fiber cladding, but for CVI/HNS tube specimen, Deck, Rohmer, kim and other researchers have conducted experiments to measure the changes of axial and hoop UTS with different fiber orientation. The results showed that the axial and hoop UTS of CVI/HNS cladding was about 462.7 MPa and 63 MPa respectively when the fiber orientation was ±30°. However, Kim's work shows that the hoop strength would be enhanced by 15% if the fiber orientation is increased from ±45° to ±65°, which means that increasing the fiber winding angle will enhance the hoop UTS, but decrease the axial strength instead.

2.1.7. Corrosion

The SiC matrix would be the first layer to contact coolant dissolution if no environmental barrier coating (EBC) to protect it. It's clear that the SiC matrix has dissolution phenomenon in LWR environment according to previous reports [53,54,64,65,85 88]. This oxidation behavior will begin at the grain boundary and occurred throughout the surface, then the grain became thinner

and finally detached from the surface, even for the pre-oxidized SiC specimens in Jeong-Yong Park's out-pile study [64]. Kim et al. has revealed that this phenomenon was irrespective of the SiC manufacturing route [54]. The most important factor that effect this process is the dissolved oxygen. Furthermore, neutron irradiation, pH value of the coolant, electrochemical potential can also accelerate this process. The possible correlation as Eq. (11) shows can describe how does the SiO_2 protective dissolve easily in hot water.

$$SiO^2 + H_2O \rightarrow H_2SiO_3^- + H^+ \rightarrow SiO_3^{2-} + 2H^+ \quad (11)$$

Jeoong-Yong Park et al. [73] conducted an experiment on long-term dissolution behavior under normal PWR simulated environment. The data was consistent with a 3 month-long experiment conducted by Chad M. Parish et al. [70] in a PWR simulated environment. the Ph value was set as 6.5, the DO concentration was 5 ppb and the water temperature was 360 °C, the experiment was conducted for 90 days. D. Kim et al. also conducted experiments to reveal the phenomenon of SiC dissolution in PWR-simulating environment. They found that the weight loose of the pre-oxidized specimen was higher in the beginning but showed a trend similar to the as-ground one. The data is redrawn in Fig. 2. The dissolution rate in PWR-simulating loop was found be linear approximately, which reaches an agreement with the conclusion of Hideo Hirayama [53] and no acceleration behavior was observed in the test [64].

According to the experiment conducted by Sosuke Kondo [74], the dissolution rate of SiC in in-pile environment will be accelerated. In his work, the dissolution was divided into two parts, hydrothermal part and irradiation enhanced part. The irradiation temperature of the specimens is 400 or 800 °C to prevent the irradiation damage recovery from high temperature, then he conducted the dissolution test on high purity SiC in hot water under irradiation condition (320 °C, 20 MPa, up to 2.6 DPA). The rates of irradiation enhanced part are redrawn in Fig. 3.

Dissolution of the SiC in hot water would bring a lot of problems and secondary consequences. A loss of cladding matrix in a long-term may expose the interphase layer or fiber layer to the coolant and lead to a degradation of the composite's mechanical properties. Since the SiO_2 dissolves in the coolant water, once its concentration excesses the saturation point, the redundant SiO2 may deposit on the coolant channels or relevant subassemblies. Even though the dissolution of SiC and its acceleration under irradiation condition have been reported and some institutions, such as MIT [63], have

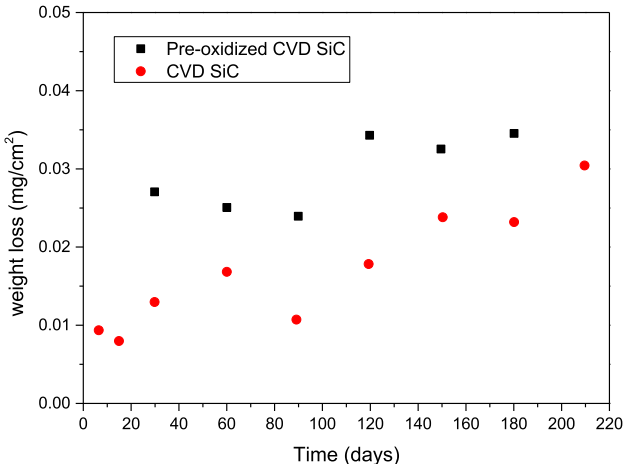

Fig. 2. Hydrothermal weight loss in 360 °C water with dissolved hydrogen control against time.

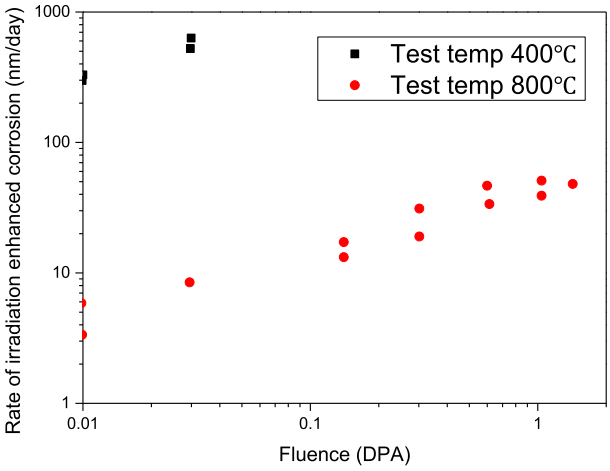

Fig. 3. Rate of irradiation enhanced corrosion part versus neutron fluence.

conducted experiments on this phenomenon, the data of is still very limited in published papers, the knowledge of this area is still very swallow, further works about identifying the mechanism and quantifying the kinetics are very necessary.

2.2. FeCrAl material

2.2.1. Overview

As a candidate cladding material for LWR to instead the Zr cladding for its limitation of oxidation at high temperature, the iron-based FeCrAl has been investigated with success experience on some industries area that high temperature oxidation resistance is needed such as water-vapor containing environments in fossil fuel energy plants [89-91]. Besides, this material was also proposed to be used as a coating material on traditional cladding surface to protect the cladding from water corrosion. The idea that applicate this material in nuclear field can date back to 1960's when General Electric conducted experiments for investigating its behaviors of corrosion and irradiation. This ferritic alloy has been improved that it has a highly improved oxidation resistance after been added with aluminum and chromium, which is strongly dependent on the contents of the chromium and the aluminum additions. However, it's not enough to be a nuclear grade material. Maintaining sufficient mechanical strength in LWR environment, good irradiation tolerance, be formable that can be made into thin wall cladding are all necessary factors, especially under BDBA scenarios. Therefore, further researches are still needed for applicating its characteristic in nuclear power generation. Some researchers have proposed that this class of FeCrAl alloys have potential capabilities that can provide more safety margin and more time to mitigate further critical results in sever accident scenarios based on their simulations. For example, L.J. Ott et al. [11] and Robb et al. [91] have indicated that the FeCrAl cladding could delay the onset of lower head dry out and extend the coping time from 4 h to 8.5 h in a simulation of short-term station black-out accident via MELCOR code.

The nuclear grade FeCrAl is mainly investigated and modified by ORNL, which is once a pioneer for the development of steel cladding with high oxidation resistance. The global research team involved Michigan university and Los Alamos National Laboratory (LANL) also focused on the improvement on the material's neutron adsorption. The research conducted by Massey et al. [92] investigated the burst behavior of FeCrAl cladding under LOCA condition and revealed that Zircaloy cannot suffer temperatures in excess of 1200 K at working condition but FeCrAl cladding can endure 1500 K

and slow down the rate of accident processes and fuel degradations.

As previous mentioned, the contents of the additional metal materials effect the in-pile performance of the cladding significantly. Higher content of Cr in the alloy can be beneficial for the high temperature oxidation resistance via supporting the stability of Al_2O_3 [93], no matter in hot water or steam environment. However, its existence would bring potential embrittlement to the alloy under normal operation temperature [94]. Higher Al content would also enhance the cladding antioxygen performance due to formation of protective Al_2O_3 on the cladding surface in team environment but increases the difficulty of cladding manufacture [95]. Yttrium, which was easily evaporated during the arc-melting process, is also be added to enhance the oxidation resistance and improve the adherence[本] the specific weight percent of composites are different in different types of FeCrAl alloy. Overall, the nominal compositions of Model FeCrAl alloys are Fe (Bal.)-Cr (10–20%)-Al (3–5)-Y (0–0.12). The nominal compositions of a typical model FeCrAl alloy and commercial FeCrAl alloys were summarized in Table 1, Mo, C, Nb etc. minor additions are mixed in the model FeCrAl alloys and to furtherly promote the thermo-mechanical performance (such as tensile strength at high temperature) while remain or minimize the negative effect to the original advantages (such as oxidation resistance or fabricability). Since there are too many kinds of FeCrAl alloys according to different compositions, the thermophysical and mechanical properties of two kinds of FeCrAl alloys that emphasically reviewed in this paper were from ORNL, the one reported in the simulation by L.J. Ott. et al. consists of Fe, 20.5–23.5% Cr, 5.8% Al, 0.08% C, 0.4% Mn and 0.7%Si, the other one reported in K.A.Gamble's investigation is C35 M, whose composition was mentioned in Table 1. But there is still some common characteristics for FeCrAl alloys with different minor additions [47]. It was found that the tensile properties were insensitive to alloy composition, the oxidation resistance in high temperature (around 1200 °C) was highly dependent on the contents of Cr and Al. After mixed with minor Mo and Nb additions, the tensile properties of the alloy (C35MN) was improved and its thermal stability was remained at the same time.

2.2.2. Thermal conductivity

Reported by L.J. Ott. et al. [11], the out-pile thermal conductivity of FeCrAl alloy used in his preliminary assessment coincides the correlation as Eq. (12) shown and is almost same compared with Zr cladding at temperature range from 300 K to 2800 K.

$$k = 2.993 + 0.03T - 1.8429 \times 10^{-5}T^2 + 7.1965 \times 10^{-9}T^3 \quad (12)$$

where K is the thermal conductivity (W/k·m); T is the cladding temperature(K).

In K.A.Gamble's investigation on the performance of FeCrAl cladding [96], the absent thermal property data of C35 M was substituted by the APMT material and provided by its manufacturer [97] as Eq. (13) shown.

$$k = 3.72 + 0.024T - 7.2 \times 10^{-6}T^2 + 1.56573 \times 10^{-9}T^3 \quad (13)$$

where K is the thermal conductivity (W/k·m); T is the cladding temperature(K). These two kinds of FeCrAl alloys have similar out-pile thermal conductivities compared with traditional Zr cladding and these parameters go up as the temperature increase. However, the data of irradiation introduced thermal properties is still limited in public literatures, relevant experiments are still needed in further work.

2.2.3. Specific heat

The specific heat of FeCrAl has been also reported by L.J. Ott. et al. and K.A. Gamble in their simulation, the specific correlations are shown in Eq. (14) and Eq. (15).

$$\begin{cases} C_p = -211.55 + 3.7854T - 6.227 \times 10^{-3}T^2 + 3.63774 \times 10^{-6}T^3 & T \le 854K \\ C_p = 2113.39 - 2.543T + 1.12 \times 10^{-3}T^2 & 854K < T \le 991K \\ C_p = 208.78 + T - 6.86 \times 10^{-4}T^2 + 1.7173 \times 10^{-7}T^3 & 991K < T \le 1776K \end{cases} \quad (14)$$

$$\begin{cases} C_p = 330.2 + 0.538T - 1.22 \times 10^{-4}T & 300 \le T \le 880K \\ C_p = 885 - 0.2T & 880K < T \le 1080K \\ C_p = 393.43 + 0.387T - 1.22 \times 10^{-4}T^2 & 1080 < T \le 1500K \end{cases} \quad (15)$$

where C_p is the specific heat (J/kg·K); T is the cladding temperature (K). Compared with traditional Zr cladding, the specific heat of FeCrAl is greater at most temperature from 300 K to 1700 K except for the phase-transition temperature of Zr alloy around 1200 K, which means that FeCrAl cladding can absorb more energy and delay the cladding temperature increasing under accident conditions. However, the neutron irradiation impact is still limited in publishes, further relevant experiments are necessary.

Table 1
The nominal compositions of a model FeCrAl alloy and commercial alloys.

ID	Fe	Cr/wt%	Al/wt%	Y/wt%	Mn/wt%	Si/wt%	Zr/wt%	Mo/wt%	Hf/wt%	Ni/wt%	C/wt%
B105 N	Bal.	10	5	–	–	–	–	–	–	–	–
APMT	Bal.	22	5	0.2	–	0.47	0.11	2.45	0.17	0.18	0.04
Alkrothal 14	Bal.	15	4	–	0.2	0.17	0.12	–	–	0.11	0.03
YHf	Bal.	20	6	0.06	0.19	0.19	0.05	–	–	0.14	0.02
C35 M	Bal.	13	4.5	0.15	–	0.2	–	2	–	–	–

2.2.4. Thermal expansion

The thermal expansion correlation of FeCrAl alloy from the simulation by L.J. Ott. et al. is as shown in Eq. (15). In K.A.Gamble's study, he used the mean thermal expansion values of APMT [97], whose thermal expansion data can also be found in another publication [98] and shown in Eq. (16), to substitute that of C35 M alloy.

$$\Delta l/l = -2.48 \times 10^{-3} + 5.623 \times 10^{-6}T + 8.44 \times 10^{-9}T^2 + 8.299 \times 10^{-13}T^3 \quad (16)$$

$$\Delta l/l = -1.733 \times 10^{-4} + 1.812 \times 10^{-5}T + 1.182 \times 10^{-9}T^2 + 1.038 \times 10^{-12}T^3 \quad (17)$$

where $\Delta l/l$ is the thermal expansion, T is the cladding temperature (K) range from 300 K to 1700 K.

The thermal expansion of FeCrAl is greater than traditional Zr cladding, which means that the gap between cladding and pellets would be larger, the process of gap closure would delay and the gap conductance would be reduced. Therefore, the fuel rod temperature at beginning of life would decrease until the gap begins to close. In other hand, this phenomenon would also put off and alleviate the PCMI (Pellet and Cladding Mechanical Interaction).

2.2.5. Young's modulus

The temperature dependent Young's modulus of C35 M alloy can be obtained from the study of Thompson et al. [99], the function is shown in Eq. (18). In the simulation of L.J. Ott. et al., the authors just investigated the effect of thermophysical properties under normal operation and accident conditions, the mechanical properties were neglected. Therefore, Young's modulus of APMT from Kanthal company [97] were added as a supplement and shown in Eq. (19).

$$E_T = 199 - 3.85 \times 10^{-2}T - 5.46 \times 10^{-5}T^2 \quad (18)$$

$$E_T = 219.7 - 7 \times 10^{-2}T - 2.39 \times 10^{-5}T^2 - 2.97 \times 10^{-9}T^3 \quad (19)$$

where E(T) is the Young's modulus (GPa), T is the cladding temperature(K) range from 300 K to 1200 K. Since the relevant experiment data is absent in publications, irradiation effect on for these two Young's modulus are not taken into account.

2.2.6. Ultimate tensile strength and yield strength

The temperature dependent ultimate tensile strength and yield stress correlation of APMT is redrawn and shown in Fig. 4 and that of C35 M is shown in Fig. 5. It is observed that the UTS and YS of APMT are higher than that of C35 M, the YS approaches UTS at a specific temperature (around 850 K for APMT and around 1000 K for C35 M alloy). Since the available data only covered temperature ranging from 300 K to 1000 K, K.A Gamble et al. set the YS and UTS equal to zero at the melting temperature (around 1773 K) and assumed that the decrease of the YS and UTS fitted a linear rule between 1000 K and 1773 K.

2.2.7. Thermal and irradiation creep rate

In normal operation conditions, long-term pressure, which consists of inward coolant pressure, outward internal gas pressure and outward PCMI, would lead to cladding creep phenomenon. It is a kind of plastic deformation and cannot recover, even though these pressures are less than the yield strength. Moreover, not only high temperature can promote this process, but also the neutron irradiation can accelerate this phenomenon. Terrani et al. provide the correlations of thermal and irradiation creep rate of C35 M alloy

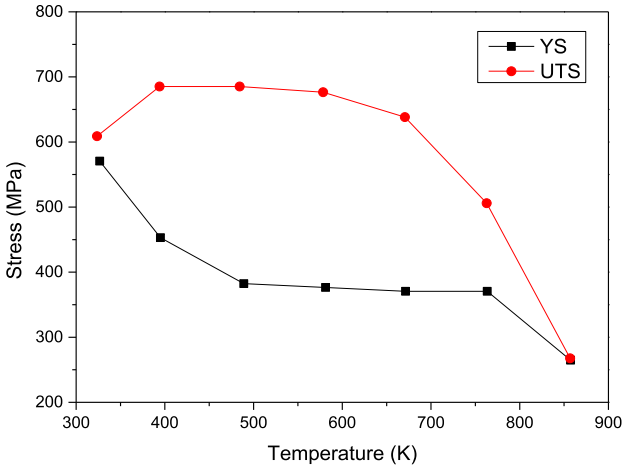

Fig. 4. YS and UTS of APMT versus elevated temperatures.

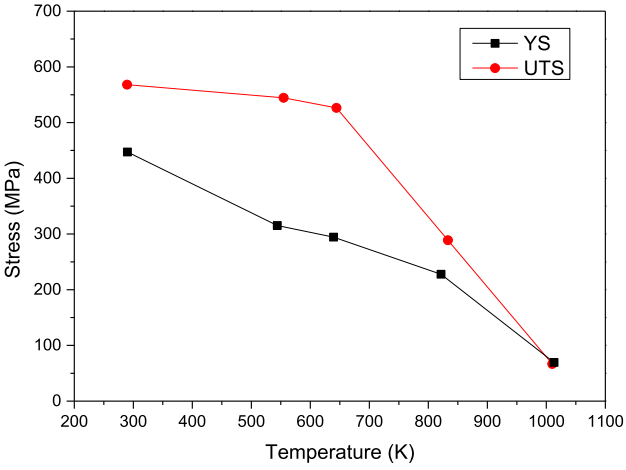

Fig. 5. YS and UTS of C35 M versus elevated temperatures.

based on recent experimental data that conducted at Halden reactor and ORNL above 873 K. The thermal creep rate below 873 K used the function provided by Sebastien Dryepondt et al. [100], which takes the form of Norton creep law as Eq. (20) shown.

$$\begin{cases} \dot{\varepsilon} = 5.96 \times 10^{-27} \cdot \sigma^{5.5} \exp\left(\dfrac{-47136}{T}\right) & T < 873K \\ \dot{\varepsilon} = 2.89 \times 10^{-36} \cdot \sigma^{5.5} \exp\left(\dfrac{-29709}{T}\right) & T > 873K \end{cases} \quad (20)$$

where $\dot{\varepsilon}$ is the thermal creep rate (s^{-1}), σ is the cladding stress (Pa) and T is the cladding temperature (K).

Based on the in-pile experiment results from ORNL, the irradiation creep coefficient satisfied the function as shown in Eq. (21).

$$\dot{\varepsilon} = 4.5 \times 10^{-31} \cdot \sigma \cdot \phi \quad (21)$$

where $\dot{\varepsilon}$ is the irradiation creep rate (s^{-1}), σ is the cladding stress (MPa) and ϕ is the effective neutron flux (neutrons/$m^2 \cdot s$).

The thermal creep rate of commercial APMT alloy is reported by its manufacturer and is shown in Table .2. The creep rates are

Table 2
The secondary creep rate at various stress levels.

Creep rate	Temperature/Stress				
s^{-1}	800 °C/MPa	900 °C/MPa	1000 °C/MPa	1100 °C/MPa	1200 °C/MPa
1e-10	20.7	12.7	7	3	1.2
1e-8	25.5	18	13	6.9	3
1e-6	30.8	25.5	22.2	16.2	7.3

constants and temperature range from 800 °C to 1200 °C. However, further data of thermal and irradiation creep rate of another kinds of cladding is limited and even the existed data are still needed to be extended and validated by further experiments, especially in neutron irradiation environment.

2.2.8. Corrosion

FeCrAl is an alumina former, which means that the alloy forms a dense and slow growing Al_2O_3 protective layer (the oxide scale of APMT is almost pure Al_2O_3) and the layer can provide several major advantages, such as slow growth rate, scale adherence, chemical stability in water environment etc. The temperature needed for form the oxidation layer is 700 °C for APMT. It is clear that there is no critical temperature range where oxidation rate is highly accelerated [98]. In theory, the oxidation kinetics of FeCrAl alloys have similar form with Zr alloys as shown in Eq. (22).

$$w^2 = k_p \times t \tag{22}$$

where represents the oxide thickness (cm), k_p is the parabolic rate constant ($g/cm^2 \cdot h^{0.5}$), t is the time(h).

The FeCrAl alloy that investigated by L.J. Ott et al. provided the parabolic rate constants at elevated temperature, which satisfied a power function as shown in Fig. 6.

The thickness of the Al_2O_3 layer can be given by Eq. (23).

$$\delta = \frac{w}{\rho} \tag{23}$$

where δ is the oxide layer thickness (cm), ρ is the density of oxygen in chromite (g/cm^3). The value for C35 M alloy that used in BISON code simulation by K.A. Terrani [101] is 3.96×10^{-3} $mg/cm^2 \cdot h^{0.5}$ for PWR and followed in K.A. Gamble's simulation. The oxidation data of commercial APMT in elevated temperatures were provided by Bo Jönsson et al. and shown in Fig. 7. The data provides the oxide layer thickness directly and satisfied power functions. It should be noted

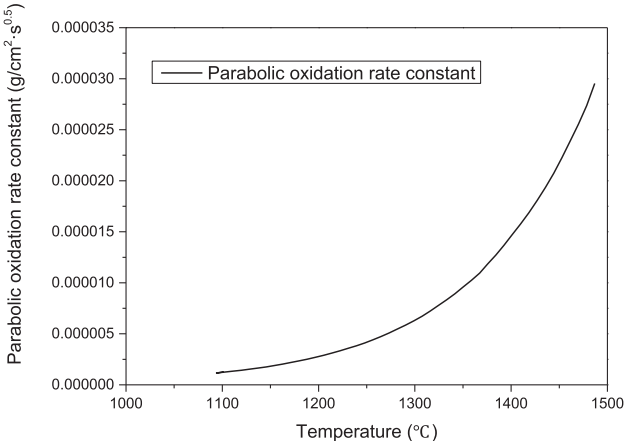

Fig. 6. Parabolic oxidation rate constant versus temperature.

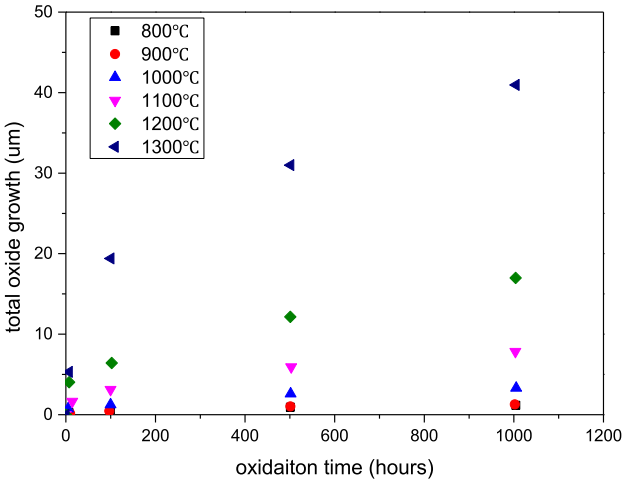

Fig. 7. Total oxide growth of APMT at elevated temperature versus time.

that in the experimental research of K.A. Terrani et al. the corrosion behavior of FeCrAl alloys in LWR coolant environment under operation condition was explored. They found that the FeCrAl exhibits slightly mass loss in hydrogen water chemistries in PWR operation environment. There are Fe-rich spinel crystals that are generated on the outer surface and will dissolved in the water. But the maximum thickness loss after one year in their environment was about 2 μm and is inconsequential for the fuel cladding application.

2.3. Ti_3SiC_2 material

2.3.1. Overview

In 1960s, Max phases materials were found and reviewed by Nowotny and his co-workers, whose researches revealed over 100 kinds of new nitrides and carbides. Generally, MAX phases compounds have a formula of $M_{n+1}AX_n$, where M is a transition metal [102], N is 1,2,3, A is an A-group element, X is C or N. Funded By National Science Foundation, Michel W. Barsoum and his co-workers showed that these phases can be described as so-called thermodynamically stable nanolaminates and represent a new class of solids. This kind of materials can be divided into 3 groups according to their stoichiometric structures, which are known as 211,312 and 413 [103]. Particularly, they have both ceramic and metallic phases and will exhibit different characteristics in these two phases. Larger hardness, higher resistance to oxidation and being more stable at high temperature are shown in ceramic phase. More resistance to thermal shock resistance, higher thermal and electrical conductivity, more machinability will be exhibited in metallic phase [103–106]. MAX phase materials combined these great characteristics together and become a kind of transition material. As a result, this kind of materials have got a lot of attention for their special combination of physical properties. In thermal physical view, they have good oxidation resistance, high melting point (over 1700 °C) and high thermal conductivity. Mechanically,

these kinds of materials have relevant low density, good thermal shock resistance, high elastic modulus and damage tolerance. In addition, the machinability of MAX phase materials is also simple [107–109], they can be machined by high speed tools bits or hack saws, even without lubrication or cooling. However, just like in the case of metals, the machining occurs by the breaking off of tiny microscopic flakes instead of by plastic deformation. Based on these advantages, the application of MAX phases materials in the nuclear area is becoming attractive with the rise of the researches on ATFs. One of the most typical MAX phase materials is the Ti_3SiC_2, which is also the best-characterized ternary to date and very interesting for nuclear application. In this article, we reviewed the thermophysical properties and the mechanical properties of Ti_3SiC_2 to facilitate the understanding and simulation of this material in nuclear area.

2.3.2. Thermal conductivity

In 1998, M.W. Barsoum et al. [110] conducted an out-pile experiment to measure the thermal conductivity of Ti_3SiC_2 range from 25 °C to 1200 °C. The results showed that the thermal conductivity was a weak function of temperature and was satisfied following correlation via least squares fitting.

$$K = 38.6 - 0.0045 \cdot T \tag{24}$$

where K is the thermal conductivity (W/m·K), T is the temperature (K).

The thermal conductivity of this material as fuel rod cladding is higher than traditional Zr cladding (~20 W/m·K) under normal operation conditions and can provide more stable thermal performance in high temperature environment.

In addition, one of its application that proposed in nuclear area is to be added into UO_2 as the second phase to improve the heat-conducting property of the pellet. It has two advantages compared with other two competitors as the second phase, BeO and polycrystalline SiC. Its thermal conductivity at 1200 °C is about 32 W/m·K, which is higher than that of BeO and close to polycrystalline SiC. What's more, it is reported that numerous defects would be generated in SiC fiber in irradiation environment and decrease its thermal performance [79], but the irradiation defects of Ti_3SiC_2 will autonomously recover at high temperature [111].

2.3.3. Specific heat

The specific heat of Ti_3SiC_2 is also from the experiment data of M.W. Barsoum et al. which is also used in the research of Bingqing Li et al. [112]. The curve fitting of the experimental data yields following equation:

$$C_p = 164.4 - (16419/T) \tag{25}$$

where C_p is the heat capacity (J/mol·K), T is temperature(T) ranged from 25 °C to 1600 °C. Since the molar mass of Ti_3SiC_2 is 195.72 kg/mol, the specific heat of Ti_3SiC_2 is:

$$C_p = 0.84 - (83.89/T) \tag{26}$$

where C_p is the specific heat (J/kg·K), T is temperature (T).

2.3.4. Coefficient of thermal expansion

The volume CTE (8.9×10^{-6}/°C), CTE in *a*-direction (8.6×10^{-6}/°C) and in c-direction (9.75×10^{-6}/°C) were calculated from the experiments, which were conducted at High Flux Isotope Reactor (HFIR) in the HB-4 via High temperature neutron diffraction measurement, by M.W. Barsoum and his co-workers. However, the coefficients were temperature independent in research of M.W.Barsoum. Bingqing Li et al. [112] provided temperature dependent CTE in their Ti_3SiC_2/UO_2 composite pellets research, the experiment results were redrawn and linear fitted in Fig. 8. The linear fitting correlation is shown in Eq. (27).

$$CTE = 0.0019 \cdot T + 7.263 \tag{27}$$

where CTE is the coefficient of thermal expansion (10^{-6}/K), T is the temperature (°C) ranged from room temperature to 1000 °C.

2.3.5. Young's modulus

Generally, MAX phase materials are quite stiff and the Young's modulus of Ti_3SiC_2 is higher than traditional Zircaloy cladding material. At room temperature, the Young's moduli is greater than 300 GPa, even higher than that of FeCrAl and SiC material. P. Finkel and other authors provided the experiment data of Young's modulus of Ti_3SiC_2 at low temperature [104]. Based on their data, the Young's modulus will decease linearly with increasing temperature as shown in Eq. (28).

$$E = E_{RT} \cdot [1 - \omega_E \cdot (T - 298)] \tag{28}$$

where E is the Young's modulus (GPa, >125 K), E_{RT} is Young's modulus at room temperature (GPa) which is 333 GPa for 3–5 μm grains and 339 GPa for 100–300 μm grains, ω_E is the temperature dependence of the appropriate modulus which is 0.88 for 3–5 μm grains and 0.75 for 100–300 μm grains.

Y.W. Bao et al. also provided the temperature dependent Young's modulus of Ti_3SiC_2 ranged from room temperature to 1200 °C, the data is shown in Fig. 9.

It's observed that the Young's modulus decreases linearly and slightly below 1000 °C, but slope becomes sharp when the temperature higher than 1000 °C and the modulus is lower than 100 GPa at 1200 °C.

2.3.6. Tensile properties

The tensile properties experiments were conducted by M. Radovic and his co-workers in 1999, the experiment temperature ranged from room temperature to 1300 °C. The mechanical response of Ti_3SiC_2 changed from brittle to plastic was observed in the experiment at around 1100 °C. Since the material is brittle below 1100 °C, the yield stress can be treated as ultimate stress, relevant correlation is shown in Eq. (29).

$$\sigma_u = -0.092 \cdot T + 223.42 \tag{29}$$

where σ_u is the ultimate stress (MPa), T is the temperature (°C)

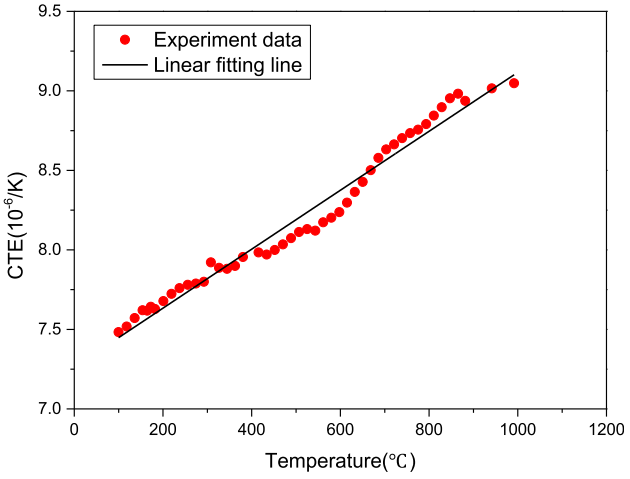

Fig. 8. The CTE of Ti_3SiC_2 versus temperature ranged from 25 °C to 1000 °C.

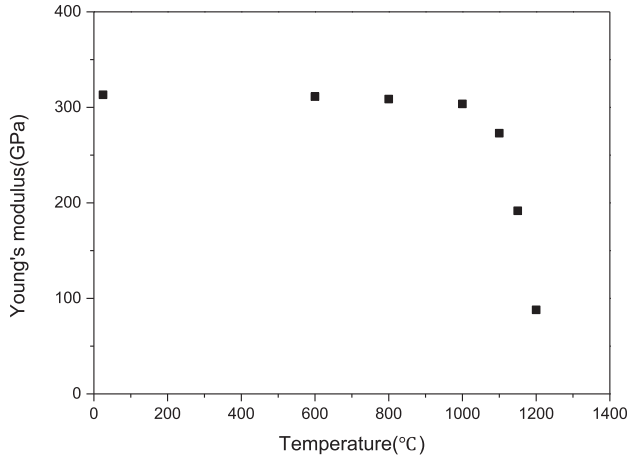

Fig. 9. Young's modulus of Ti_3SiC_2 versus temperature.

ranged from room temperature to 1100 °C. The failure strain is zero. When temperature is above 1100 °C, the ultimate stress decreases rapidly and coincides Eq. (30) as follows:

$$\sigma_u = -0.521 \cdot T + 693.86 \tag{30}$$

where σ_u is the ultimate stress (MPa), T is the temperature (°C) ranged from 1100 °C to 1300 °C. In this temperature range, the material becomes plastic and the failure strain will increase that yield the correlation below:

$$\varepsilon_f = 0.00102 \cdot T - 1.1468 \tag{31}$$

where ε_f is the failure strain, T is the temperature (°C) ranged from 1100 °C to 1300 °C.

2.3.7. The second creep rate

The secondary creep rate of Ti_3SiC_2 satisfies the unified equation form and often express as:

$$\dot{\varepsilon} = A\sigma^n \exp\left(\frac{-Q}{RT}\right) \tag{32}$$

where $\dot{\varepsilon}$ is the secondary creep rate (s^{-1}), σ is the stress (MPa), Q is the activation energy (J/mol), n is the stress exponent, T is the temperature (K), A is a constant, R is the gas constant. Relevant parameters of Ti_3SiC_2 was measured by M.W. Barsoum et al. and shown in Eq. (33):

$$\dot{\varepsilon} = 2.2 \times 10^7 \sigma^{1.15} \exp\left(\frac{-420 \pm 15 kJ/mol}{RT}\right) \tag{33}$$

The range of temperature in this experiment is from 1000 °C to 1200 °C and the stress is from 10 MPa to 100 MPa. Y.W. Bao [113] also conducted the experiment to investigate the relationship between creep and the stress via bending test. It turns out that the creep is insensitive to the temperature below around 1000 °C while increases markedly when the temperature is above 1050 °C, which is also the transition temperature from brittle to ductile.

2.3.8. Corrosion

The overall process function of oxidation reaction in air is:

$$Ti_3SiC_2(s) + O_2(g) \rightarrow TiO_2(s) + SiO_2(s) + (CO(g) \text{ or } CO_2(g)) \tag{34}$$

The formed scale is dense, adhesive and layered. Besides, the oxidative scale also has resistance to the thermal cycling. The inner layer is the mixture of SiO_2 and TiO_2 and the outer layer is the TiO_2. These characteristics ensure that the material has a strong oxidation resistance to the air. The parabolic kinetics in air, Kp, increased with the increasing temperature, but can be ignored below 900 °C [114]. The relevant data is listed in Table 3.

What's more important for application of Ti_3SiC_2 in nuclear area is its hydrothermal oxidation performance in hot water. Haibin Zhang and his co-workers [115] conducted the experiment to investigate it in continuous water flow at temperature ranged from 500 °C to 700 °C. It turned out that the oxidation was weak below 600 °C, but accelerated at 700 °C because of the cracks in the scale. The overall oxidation reactions are:

$$\begin{aligned} &Ti_3SiC_2 + 12H_2O = 3TiO_2 + SiO_2 + 2CO_2 + 12H_2 \quad T > 550^\circ C \\ &Ti_3SiC_2 + 9H_2O = 3TiO_2 + SiO_2 + \frac{1}{2}CO_2 + \frac{3}{2}CH_4 + 6H_2 \; T < 550^\circ C \end{aligned} \tag{35}$$

The experiment data of weight gain versus time at temperature ranged from 500 °C to 700 °C were provided by Haibin Zhang et al. and redrawn in Fig. 10. The kinetic obey a linear time law, which is 1.2×10^{-2}, 2.5×10^{-2} and 24.2×10^{-2} μg/mm^2/h for temperature of 500 °C, 700 °C and 900 °C respectively.

As mentioned previously in section 2.1.7, the protective layer SiO_2 will dissolve into the water and just TiO_2 remains, which will weaken the oxidation resistance in hot water. Besides, when the temperature reaches around 700 °C, the phase transformation from anatase to rutile will result in addition tensile stress in the oxide layer for the higher density and crack the oxides. This behavior will furtherly weaken the oxidation resistance of the material in water.

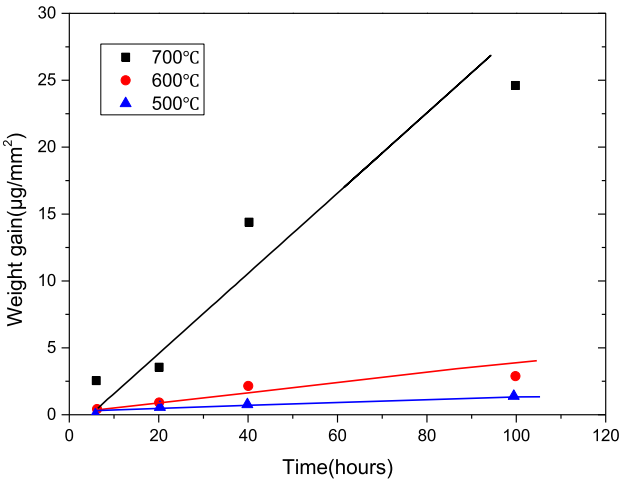

Fig. 10. Weight gain versus time in hot water at temperature of 500 °C, 600 °C and 700 °C.

Table 3
Parabolic rate constants ($kg^2 \cdot m^{-4} \cdot s^{-1}$) for the oxidation of Ti_3SiC_2.

	1000 °C	1200 °C	1300 °C	1400 °C	Activation energy (kJ/mol)
Ti_3SiC_2	1.31×10^{-8}	6.58×10^{-7}	2.7×10^{-5}	1.4×10^{-4}	320

2.4. Advantages and challenges

Main thermophysical and mechanical properties of the three potential cladding materials in nuclear application are reviewed in this paper, we intend to conclude their advantages and challenges to enhance relevant understanding and provide convenience for code simulations based on experimental data. They all have much higher accident tolerance compared with traditional zircaloy cladding, but they are still facing their particular problems and challenges in practical applications.

SiC_f/SiC composite cladding has small neutron absorption cross sections, great stability, stronger mechanical performance and better thermophysical properties as mentioned above. However, dissolution behavior in hot water (PWR under normal condition is a typical environment) is the first problem. This behavior can lead to SiO_2 deposition on joints and channels. Thinner outer layer of the cladding will decrease the possibility of providing sufficient protection for the middle composite layer. Current solution is to spray an EBC on the cladding surface, but relevant research and technology is still immature. What's more, experiments revealed that its thermal conductivity will decrease to a very low value after neutron irradiation. This phenomenon is dependent on manufacturing process and can be alleviated via techniques promotion.

FeCrAl is often designed as a kind of monolithic cladding material, but also be proposed as a kind of surface coating material. It has great stability in water or stream environment, much less hydrogen production and stronger mechanical stress, relevant researches on it are also relative sufficient. However, its neutron economy is lower than zircaloy and has no advantages in thermal performance. Aim at these problems, reducing the cladding thickness is a potential solution. Besides, higher thermal expansion can lead to larger gap thickness and promote the pellets temperature, reducing cladding thickness can also improve its thermal performance. Specific value is needed to be ascertained via simulations and experiments.

Ti_3SiC_2 is a representative of MAX phase material, it is a potentially suitable cladding material or coating material based on its out-pile behavior. Its higher thermal conductivity, higher melting point and good tensile properties all make it attractive in nuclear application. However, some researches revealed that this material has limitations for application in LWR. Its oxidation resistance will be reduced in hydrothermal environment and its oxidation behavior in high temperature steam environment is still unknow. Besides, it has outward diffusion problems of fission products (Cs and Ag) at elevated temperature [116]. Its in-pile properties is also limited in publications. Inner and outer coating may alleviate the diffusion and dissolution problem, further in-pile experiments are very necessary before further researches.

3. Conclusion

Full SiC_f/SiC cladding, FeCrAl and MAX phase Ti_3SiC_2 are three potential cladding materials for ATF design in a pressurized water reactor, no matter in thermohydraulic or mechanical view. Though the physical parameters and correlations that reviewed in this article, it is observed that their stronger elastic properties, stronger creep resistance and higher ultimate stresses can provide better protective capability mechanically and remain the fabricated structure, especially in the case of RIA when PCMI threat the safety of the cladding. Their higher specific heat, stronger oxidation resistance and higher thermal conductivity are conductive to delay the temperature rise and provide more coping time. However, commercial applications for these three new cladding are still facing many critical application problems. Relevant details are described in above sections. After all, there is still a certain distance to the commercial application of these new ATF claddings. Many significant properties, especially in-pile physical properties, still lack in publications, it will bring much inconvenience to simulation works. Our review work will continually pay attention on relevant researches.

Acknowledgement

This research was supported by the National Natural Science Foundation of China (Grant No.11575141) and also supported by Chinese “Program for Changjiang Scholars and Innovative Research Team in University” (No: IRT1280).

References

[1] F. Kamil, Fukushima nuclear accident, Decouverte (Paris) 1 (373) (2011) 28–31.
[2] J. Carmack, F. Goldner, S.M. Bragg-Sitton, L.L. Snead, Overview of the US DOE accident tolerant fuel development program, in: Proc. 2013 LWR Fuel Performance Meeting/TopFuel, 2013, pp. 15–19.
[3] L. Soffer, S. Burson, C. Ferrell, R. Lee, J. Ridgely, Accident Source Terms for Light-Water Nuclear Power Plants. NUREG-1465 6, U.S.NRC, Washington, DC, United States, 1995.
[4] F. Goldner, Development Strategy for Advanced LWR Fuels with Enhanced Accident Tolerant, Enhanced Accident Tolerant LWR Fuels National Metrics Workshop 2012, 2012 (Germantown, MD, United States).
[5] S. Bragg-Sitton, Development of advanced accident-tolerant fuels for commercial LWRs, Nucl. News 57 (2014) 83.
[6] S. Chu, A. Majumdar, Opportunities and challenges for a sustainable energy future, Nature 488 (2012) 294–303.
[7] K.R. Gurney, D.L. Mendoza, Y. Zhou, M.L. Fischer, C.C. Miller, S. Geethakumar, S. dela Rue du Can, High resolution fossil fuel combustion CO2 emission fluxes for the United States, Environ. Sci. Technol. 43 (2009) 5535–5541.
[8] Y.-H. Koo, J.-H. Yang, J.-Y. Park, K.-S. Kim, H.-G. Kim, D.-J. Kim, Y.-I. Jung, K.-W. Song, KAERI's development of LWR accident-tolerant fuel, Nucl. Technol. 186 (2014) 295–304.
[9] B.A. Pint, K.A. Terrani, M.P. Brady, T. Cheng, J.R. Keiser, High temperature oxidation of fuel cladding candidate materials in steam–hydrogen environments, J. Nucl. Mater. 440 (2013) 420–427.
[10] K. Yueh, K.A. Terrani, Silicon carbide composite for light water reactor fuel assembly applications, J. Nucl. Mater. 448 (2014) 380–388.
[11] L.J. Ott, K.R. Robb, D. Wang, Preliminary assessment of accident-tolerant fuels on LWR performance during normal operation and under DB and BDB accident conditions, J. Nucl. Mater. 448 (2014) 520–533.
[12] N.M. George, K. Terrani, J. Powers, A. Worrall, I. Maldonado, Neutronic analysis of candidate accident-tolerant cladding concepts in pressurized water reactors, Ann. Nucl. Energy 75 (2015b) 703–712.
[13] F. Goldner, Development Strategy for Advanced LWR Fuels with Enhanced Accident Tolerant, Enhanced Accident Tolerant LWR Fuels National Metrics Workshop 2012,Germantown, MD, United States, 2012.
[14] J. Wang, M. Mccabe, L. Wu, et al., Accident tolerant clad material modeling by MELCOR: benchmark for SURRY short term station black out, Nucl. Eng. Des. 313 (2017a) 458–469.
[15] J. Wang, H.J. Jo, M.L. Corradini, et al., “Potential recovery actions from a severe accident in a PWR: MELCOR analysis of a station blackout scenario”, Nucl. Technol. 204 (1) (2018) 1–14.
[16] J. Wang, H.J. Jo, M.L. Corradini, Accident Tolerant Fuel (ATF) Coating and Cladding Thermal Hydraulic Properties Evaluation by MELCOR YU 1.8.6: Benchmark for SURRY Short Term Station Black Out. 2018 ANS Annual Meeting, 2018. June 17-21, Philadelphia, PA, United States.
[17] J. Wang, A. Gurgen, M.L. Corradini, et al., Accident tolerant fuel benchmark calculation by MELCOR and TRACE for a simplified generic pressure water reactor. 2018, in: International Congress on Advances in Nuclear Power Plants, 2018. April.8-11, Charlotte, NC, United States.
[18] M.N. Chong, S. Lei, B. Jin, C. Saint, C.W. Chow, Optimisation of an annular photoreactor process for degradation of Congo Red using a newly synthesized titania impregnated kaolinite nano-photocatalyst, Separ. Purif. Technol. 67 (2009) 355–363.
[19] P. Hofmann, S.J. Hagen, V. Noack, G. Schanz, L.K. Sepold, Chemical-physical behavior of light water reactor core components tested under severe reactor accident conditions in the CORA facility, Nucl. Technol. 118 (1997) 200–224.
[20] D. Squarer, A. Pieczynski, L. Hochreiter, Effect of debris bed pressure, particle size, and distribution on degraded nuclear reactor core coolability, Nucl. Sci. Eng. 80 (1982) 2–13.
[21] S.J. Zinkle, K.A. Terrani, J.C. Gehin, L.J. Ott, L.L. Snead, Accident tolerant fuels for LWRs: a perspective, J. Nucl. Mater. 448 (2014) 374–379.
[22] K.A. Terrani, S.J. Zinkle, L.L. Snead, Advanced oxidation-resistant iron-based alloys for LWR fuel cladding, J. Nucl. Mater. 448 (2014b) 420–435.
[23] S.J. Zinkle, G. Was, Materials challenges in nuclear energy, Acta Mater. 61

(2013) 735–758.
[24] G. González-Doncel, O. Sherby, High temperature creep behavior of metal matri Aluminum SiC composites, Acta Metall. Mater. 41 (1993) 2797–2805.
[25] A. Evans, C. Padgett, R. Davidge, Strength of pyrolytic SiC coatings of fuel particles for high- temperature gas- cooled reactors, J. Am. Ceram. Soc. 56 (1973) 36–41.
[26] M. Ben-Belgacem, V. Richet, K.A. Terrani, Y. Katoh, L.L. Snead, Thermo-mechanical analysis of LWR SiC/SiC composite cladding, J. Nucl. Mater. 447 (2014) 125–142.
[27] M. Baba, Fukushima accident: what happened? Radiat. Meas. 55 (2013) 17–21.
[28] P.C. Burns, R.C. Ewing, A. Navrotsky, Nuclear fuel in a reactor accident, Science (Washington, D.C.) 335 (2012) 1184–1188.
[29] N. Kinoshita, K. Sueki, K. Sasa, J.-i. Kitagawa, S. Ikarashi, T. Nishimura, Y.-S. Wong, Y. Satou, K. Handa, T. Takahashi, Assessment of individual radionuclide distributions from the Fukushima nuclear accident covering central-east Japan, Proc. Natl. Acad. Sci. 108 (2011) 19526–19529.
[30] J.M. Schwantes, C.R. Orton, R.A. Clark, Analysis of a nuclear accident: fission and activation product releases from the Fukushima Daiichi nuclear facility as remote indicators of source identification, extent of release, and state of damaged spent nuclear fuel, Environ. Sci. Technol. 46 (2012) 8621–8627.
[31] B.B. Wittneben, The impact of the Fukushima nuclear accident on European energy policy, Environ. Sci. Policy 15 (2012) 1–3.
[32] K. Barrett, S. Bragg-Sitton, D. Galicki, Advanced LWR Nuclear Fuel Cladding System Development Trade-Off Study. INL/EXT-12-27090, INL External Report, 2012 (Idaho Falls, ID, United States).
[33] B.A. Pint, K.A. Terrani, Y. Yamamoto, L.L. Snead, Material selection for accident tolerant fuel cladding, Metall. Mater. Trans. A 2 (2015) 190–196.
[34] J.-Y. Park, I.-H. Kim, Y.-I. Jung, H.-G. Kim, D.-J. Park, B.-K. Choi, High temperature steam oxidation of Al 3 Ti-based alloys for the oxidation-resistant surface layer on Zr fuel claddings, J. Nucl. Mater. 437 (2013b) 75–80.
[35] S. Ray, E. Lahoda, F. Franceschini, Assessment of Different Materials for Meeting the Requirement of Future Fuel Designs, Reactor Fuel Performance Meeting, 2012, pp. 2–6. Paper A.
[36] M.C. Teague, B.S. Fromm, M.R. Tonks, D.P. Field, Using coupled mesoscale experiments and simulations to investigate high burn-up oxide fuel thermal conductivity, JOM (J. Occup. Med.) 66 (2014) 2569–2577.
[37] M. Tonks, D. Schwen, Y. Zhang, P. Chakraborty, X. Bai, B. Fromm, J. Yu, M. Teague, D. Andersson, Assessment of MARMOT: A Mesoscale Fuel Performance Code, Idaho National Laboratory (INL), Idaho Falls, ID, United States, 2015.
[38] K. Metzger, T. Knight, R. Williamson, Model of U_3Si_2 fuel system using BISON fuel code. Proceedings of the International Congress on Advances in Nuclear Power Plants–ICAPP 2014, 2014 (Charlotte, NC, United States).
[39] J. Carmack, L. Braase, C. Papesch, D. Hurley, M. Tonks, Y. Zhang, K. Gofryk, J. Harp, R. Fielding, C. Knight, Thermal Properties Measurement Report, Idaho National Laboratory (INL), Idaho Falls, United States, 2015.
[40] K. Barrett, K. Ellis, C. Glass, G. Roth, M. Teague, J. Johns, Critical processes and parameters in the development of Accident Tolerant Fuel drop-in capsule irradiation tests, Nucl. Eng. Des. 294 (2015) 38–51.
[41] B. Qiu, et al., A comparative study on preliminary performance evaluation of ATFs under normal and accident conditions with FRAP-ATF code, Prog. Nucl. Energy 105 (2018) 51–60.
[42] Y.B. Deng, Y.W. Wu, B.W. Qiu, et al., Development of a new pellet-clad mechanical interaction (PCMI) model and its application in ATFs, Ann. Nucl. Energy 104 (2017) 146–156.
[43] N.R. Brown, A. Aronson, M. Todosow, R. Brito, K.J. McClellan, Neutronic performance of uranium nitride composite fuels in a PWR, Nucl. Eng. Des. 275 (2014) 393–407.
[44] V. Mehta, J.S. Cooper, Review and analysis of PEM fuel cell design and manufacturing, J. Power Sources 114 (2003) 32–53.
[45] M. Farmer, L. Leibowitz, K.A. Terrani, K.R. Robb, Scoping assessments of ATF impact on late-stage accident progression including molten core–concrete interaction, J. Nucl. Mater. 448 (2014) 534–540.
[46] B.A. Pint, S. Dryepondt, K.A. Unocic, D.T. Hoelzer, Development of ODS FeCrAl for compatibility in fusion and fission energy applications, JOM (J. Occup. Med.) 66 (2014) 2458–2466.
[47] Y. Yamamoto, B. Pint, K. Terrani, K. Field, Y. Yang, L. Snead, Development and property evaluation of nuclear grade wrought FeCrAl fuel cladding for light water reactors, J. Nucl. Mater. 467 (2015) 703–716.
[48] G.J. Youinou, R.S. Sen, Impact of accident-tolerant fuels and claddings on the overall fuel cycle: a preliminary systems analysis, Nucl. Technol. 188 (2014) 123–138.
[49] C.H. Henager Jr., W.D. Bennett, A.L. Doherty, E. Fuller, J.S. Hardy, R.P. Omberg, Corrosion Report for the U-Mo Fuel Concept, Pacific Northwest National Laboratory (PNNL), Richland, WA (US), 2014.
[50] J. Hu, D. Wolfe, A. Motta, et al., Radiation Tolerance of Multilayer (TiN, TiAlN) Ceramic ATF Coating. 2017 ANS Winter Meeting, Washington, DC, United States, 2017.
[51] Y. Zhang, D.S. Aidhy, T. Varga, S. Moll, P.D. Edmondson, F. Namavar, K. Jin, C.N. Ostrouchov, W.J. Weber, The effect of electronic energy loss on irradiationinduced grain growth in nanocrystalline oxides, Phys. Chem. Chem. Phys. 16 (2014a) 8051–8059.
[52] J. Brachet, C. Lorrette, A. Michaux, C. Sauder, I. Idarraga-Trujillo, M. Le Saux, A. Ambard, CEA studies on advanced nuclear fuel claddings for enhanced Accident Tolerant LWRs Fuel (LOCA and beyond LOCA conditions), in: Fontevraud 8, Contribution of Materials Investigations and Operating Experience to LWRs' Safety, Performance and Reliability, 2014. September 15-18, 2014, France, Avignon.
[53] K.A. Terrani, et al., Silicon carbide oxidation in steam up to 2 MPa, J. Am. Ceram. Soc. 97 (2014) 2331–2352.
[54] Y. Katoh, et al., Radiation effects in SiC for nuclear structural applications, Curr. Opin. Solid State Mater. Sci. 16 (2012) 143–152.
[55] J.-H. Chun, S.-W. Lim, B.-D. Chung, W.-J. Lee, Safety evaluation of accidenttolerant FCM fueled core with SiC-coated zircalloy cladding for design-basis-accidents and beyond DBAs, Nucl. Eng. Des. 289 (2015) 287–295.
[56] T. Koyanagi, Y. Katoh, M. Snead, SiC/SiC Cladding Materials Properties Handbook, U.S. Department of Energy-Nuclear Technology Research and Development Advanced Fuels Campaign ORNL/TM-20, 2017.
[57] A. Ellison, J. Zhang, J. Peterson, A. Henry, Q. Wahab, J. Bergman, Y.N. Makarov, A. Vorob'ev, A. Vehanen, E. Janzén, High temperature CVD growth of SiC, Mater. Sci. Eng., B 61 (1999) 113–120.
[58] H. Tsou, W. Kowbel, A hybrid PACVD SiC/CVD Si3N4SiC multilayer coating for oxidation protection of composites, Carbon 33 (1995) 1279–1288.
[59] Y. Katoh, K.A. Terrani, Systematic Technology Evaluation Program for SiC/SiC Composite Based Accident-Tolerant LWR Fuel Cladding and Core Structures: Revision 2015, Oak Ridge National Laboratory (ORNL), 2015.
[60] D.M. Carpenter, Assessment of Innovative Fuel Designs for High Performance Light Water Reactors, 2006.
[61] H. Feinroth, et al., Mechanical strength of CTP Triplex SiC fuel clad tubes after irradiation in MIT research reactor under PWR coolant conditions, Ceram. Eng. Sci. Proc. 30 (10) (2009) 47.
[62] C. Deck, et al., Characterization of SiC–SiC composites for accident tolerant fuel cladding, J. Nucl. Mater. 466 (2015) 667–681.
[63] J.D. Stempien, et al., Characteristics of composite silicon carbide fuel cladding after irradiation under simulated PWR conditions, Nucl. Technol. 183 (2013) 13–29.
[64] D. Kim, et al., Fabrication and measurement of hoop strength of SiC triplex tube for nuclear fuel cladding applications, J. Nucl. Mater. 458 (2015) 29–36.
[65] Y.I. Jung, S.-H. Kim, J.-Y. Park, Manufacturing process for the metal-ceramic hybrid fuel cladding tube, Trans. Korean Nucl. Soc. (2012) 25–26.
[66] M. Takeda, et al., Effect of hydrogen atmosphere on pyrolysis of cured polycarbosilane fibers, J. Am. Ceram. Soc. 83 (2000) 1063–1069.
[67] H. Ichikawa, Development of high performance SiC fibers derived from polycarbosilane using electron beam irradiation curing-a review, J. Ceram. Soc. Jpn. 114 (2006) 455–460.
[68] T. Ishikawa, et al., High-strength alkali-resistant sintered SiC fibre stable to 2200°C, Nature 391 (1998) 773–775.
[69] Y. Katoh, et al., Continuous SiC fiber, CVI SiC matrix composites for nuclear applications: properties and irradiation effects, J. Nucl. Mater. 448 (2014) 448–476.
[70] C. Sauder, Ceramic matrix composites: nuclear applications, Ceram. Matrix Compos.: Mater. Model. Technol. (2014) 609–646.
[71] M. Uchihashi, et al., Development of SiC/SiC composites for nuclear reactor core with enhanced safety, in: International Conference on Nuclear Engineering (ICONE) 2015.23, The Japan Society of Mechanical Engineers, 2015.
[72] C.M. Parish, et al., Microstructure and hydrothermal corrosion behavior of NITE-SiC with various sintering additives in LWR coolant environments, J. Eur. Ceram. Soc. 37 (2017) 1261–1279.
[73] J.Y. Park, et al., Long-term corrosion behavior of CVD SiC in 360 C water and 400 °C steam, J. Nucl. Mater. 443 (2013) 603–607.
[74] S. Kondo, M. Lee, T. Hinoki, Y. Hyodo, F. Kano, Effect of irradiation damage on hydrothermal corrosion of SiC, J. Nucl. Mater. 464 (2015) 36–42.
[75] Z. Duan, et al., Current status of materials development of nuclear fuel cladding tubes for light water reactors, Nucl. Eng. Des. 316 (2017) 131–150.
[76] I. Spitsberg, J. Steibel, Thermal and environmental barrier coatings for SiC/SiC CMCs in aircraft engine applications, Int. J. Appl. Ceram. Technol. (2004) 291–301.
[77] T. Maruyama, et al., Relationship between dimensional changes and the thermal conductivity of neutron irradiated SiC, J. Nucl. Mater. (2004) 329–333.
[78] L.L. Snead, Limits on irradiation-induced thermal conductivity and electrical resistivity in silicon carbide materials, J. Nucl. Mater. (2004) 524–529, 329–333.
[79] L.L. Snead, et al., Handbook of SiC properties for fuel performance modeling, J. Nucl. Mater. 371 (1) (2007) 329–377.
[80] R.H. Jones, D. Steiner, H.L. Heinisch, G.A. Newsome, H.M. Kerch, Radiation resistant ceramic matrix composites, J. Nucl. Mater. 245 (1997) 87–107.
[81] K.A. Schwetz, in: Handbook of Ceramic Hard Materials, Wiley-VCH Verlag GmbH, 2008, pp. 683–748.
[82] N. Miriyala, et al., The mechanical behavior of a Nicalon/SiC composite at room temperature and 1000°C, J. Nucl. Mater. 253 (1998) 1–9.
[83] E. Rohmer, E. Martin, C. Lorrette, Mechanical properties of SiC/SiC braided tubes for fuel cladding, J. Nucl. Mater. 453 (2014) 16–21.
[84] T. Koyanagi, Y. Katoh, Mechanical properties of SiC composites neutron irradiated under light water reactor relevant temperature and dose conditions, J. Nucl. Mater. 494 (2017) 46–54.
[85] Y. Katoh, et al., Thermophysical and mechanical properties of near-stoichiometric fiber CVI SiC/SiC composites after neutron irradiation at elevated temperatures, J. Nucl. Mater. 403 (2010) 48–61.

[86] G. Newsome, et al., Evaluation of neutron irradiated silicon carbide and silicon carbide composites, J. Nucl. Mater. 371 (2007) 76–89.
[87] T. Nozawa, et al., Determination and prediction of axial/off-axial mechanical properties of SiC/SiC composites, Fusion Eng. Des. 87 (2012) 803–807.
[88] C.K. Ang, et al., Examination of Hybrid Metal Coatings for Mitigation of Fission Product Release and Corrosion Protection of LWR SiC/SiC, Oak Ridge National Laboratory (ORNL), Oak Ridge, TN, United States, 2016.
[89] H.A. Friggens, D.R. Holmes, Nucleation and growth of magnetite films on Fe in high-temperature water, Corros. Sci. 8 (1968) 871–881.
[90] C.S. Wukusick, J.F. Collins, An iron-chromium-aluminum alloy containing yttrium, Mater. Res. Std. 4 (1964).
[91] K.R. Robb, Analysis of the FeCrAl Accident Tolerant Fuel Concept Benefits during BWR Station Blackout Accidents, Oak Ridge National Lab.(ORNL), Oak Ridge, TN, United States, 2015.
[92] C.P. Massey, K.A. Terrani, S.N. Dryepondt, et al., Cladding burst behavior of Fe-based alloys under LOCA, J. Nucl. Mater. 470 (2016) 128–138.
[93] F.H. Stott, G.C. Wood, J. Stringer, The influence of alloying elements on the development and maintenance of protective scales, Oxid. Metals 44 (1995) 113–145.
[94] J. Ejenstam, M. Thuvander, P. Olsson, et al., Microstructural stability of Fe–Cr–Al alloys at 450–550° C, J. Nucl. Mater. 457 (2015) 291–297.
[95] H.P. Qu, Y.P. Lang, C.F. Yao, et al., The effect of heat treatment on recrystallized microstructure, precipitation and ductility of hot-rolled Fe–Cr–Al–REM ferritic stainless steel sheets, Mater. Sci. Eng. 562 (2013) 9–16.
[96] K.A. Gamble, T. Barani, D. Pizzocri, et al., An investigation of FeCrAl cladding behavior under normal operating and loss of coolant conditions, J. Nucl. Mater. 491 (2017) 55–66.
[97] Kanthal APMT (tube) datasheet. http://kanthal.com/en/products/materialdatasheets/tube/kanthal-apmt/, 2012.
[98] B. Jönsson, Q. Lu, D. Chandrasekaran, et al., Oxidation and creep limited lifetime of Kanthal APMT®, a dispersion strengthened FeCrAlMo alloy designed for strength and oxidation resistance at high temperatures, Oxid. Metals 79 (2013) 29–39.
[99] Z.T. Thompson, K.A. Terrani, Y. Yamamoto, ORNL/TM-2015/, Elastic Modulus Measurement of ORNL ATF FeCrAl Alloys, vol 632, 2015, pp. 1–17.
[100] S. Dryepondt, B.A. Pint, E. Lara-Curzio, Creep behavior of commercial FeCrAl foils: beneficial and detrimental effects of oxidation, Mater. Sci. Eng., A (2012) 10–18.
[101] K.A. Terrani, B.A. Pint, Y.J. Kim, et al., Uniform corrosion of FeCrAl alloys in LWR coolant environments, J. Nucl. Mater. 479 (2016) 36–47.
[102] M.W. Barsoum, The $M_{N+1}AX_N$ phases: a new class of solids, Prog. Solid State Chem. 28 (2000) 201–281.
[103] Z. Yanchun, S. Zhimei, S. Jihong, et al., Titanium silicon carbide: a ceramic or a metal, Z Metallkd 91 (2000) 329–334.
[104] P. Finkel, M.W. Barsoum, T. El-Raghy, Low temperature dependencies of the elastic properties of Ti 4 AlN 3, Ti 3 Al 1.1 C 1.8, and Ti_3SiC_2, J. Appl. Phys. 87 (4) (2000) 1701–1703.
[105] Z. Sun, Y. Zhou, M. Li, Oxidation behaviour of Ti_3SiC_2-based ceramic at 900–1300° C in air, Corros. Sci. 43 (6) (2001) 1095–1109.
[106] R. Radhakrishnan, J.J. Williams, M. Akinc, Synthesis and high-temperature stability of Ti3SiC2, J. Alloy. Comp. 285 (1–2) (1999) 85–88.
[107] Z.M. Sun, H. Hashimoto, Z.F. Zhang, et al., Synthesis and characterization of a metallic ceramic material–Ti3SiC2, Mater. Trans. 47 (1) (2006) 170–174.
[108] T. El-Raghy, M.W. Barsoum, A. Zavaliangos, et al., Processing and mechanical properties of Ti3SiC2: II, effect of grain size and deformation temperature, J. Am. Ceram. Soc. 82 (10) (1999) 2855–2860.
[109] Y. Zhou, Z. Sun, Microstructure and mechanism of damage tolerance for Ti_3SiC_2 bulk ceramics, Mater. Res. Innov. 2 (6) (1999) 360–363.
[110] M.W. Barsoum, H.I. Yoo, I.K. Polushina, et al., Electrical conductivity, thermopower, and hall effect of Ti_3AlC_2, Ti_4AlN_3, and Ti_3SiC_2, Phys. Rev. B 62 (15) (2000) 10194.
[111] A.S. Farle, C. Kwakernaak, S. van der Zwaag, W.G. Sloof, A conceptual study into the potential of $M_{n+1}AX_n$-phase ceramics for self-healing of crack damage, J. Eur. Ceram. Soc. 35 (2015).
[112] B. Li, Z. Yang, M. Chu, et al., Ti_3SiC_2/UO_2 composite pellets with superior high-temperature thermal conductivity, Ceram. Int. 44 (16) (2018) 19846–19850.
[113] Y.W. Bao, Y.C. Zhou, et al., Mechanical properties of Ti_3SiC_2 at high temperature, Acta Metall. Sin. 17 (4) (2004) 465–470.
[114] M.W. Barsoum, T. El-Raghy, L.U.J.T. Ogbuji, Oxidation of Ti3SiC2 in air, J. Electrochem. Soc. 144 (7) (1997) 2508–2516.
[115] H. Zhang, V. Presser, C. Berthold, et al., Mechanisms and kinetics of the hydrothermal oxidation of bulk titanium silicon carbide, J. Am. Ceram. Soc. 93 (4) (2010) 1148–1155.
[116] W. Jiang, C.H. Henager Jr., T. Varga, et al., Diffusion of Ag, Au and Cs implants in MAX phase Ti3SiC2, J. Nucl. Mater. 462 (2015) 310–320.